FULL PAPER

Dalton
www.rsc.org/dalton

Synthesis, characterization and catalytic ATP-hydrolysis of two tetrairon(III) complexes bridged by succinate/terephthalate with tris(2-benzimidazolylmethyl) amine †

Dong-feng Li,[a,d] Zhan-ru Liao,*[a] Yong-ge Wei,[b] Fei Du,[c] Ming Wang,[a] Wen-xue Chen,[a] Wu-ke Li[a] and Xi-an Mao[c]

[a] *Department of Chemistry, Central China Normal University, Wuhan 430079, P. R. China. E-mail: zrliao@ccnu.edu.cn*

[b] *Department of Chemistry, Beijing University, Beijing, 100871, P. R. China*

[c] *Laboratory of NMR & Atomic Molecular Physics, Wuhan Institute of Physics and Mathematics, Chinese Academy of Sciences, Wuhan 430071, P. R. China*

[d] *State Key Laboratory of Coordination Chemistry, Nanjing University, Nanjing 210093, P. R. China*

Received 15th October 2002, Accepted 25th March 2003
First published as an Advance Article on the web 9th April 2003

Two new tetranuclear iron(III) complexes, $[Fe_4(TBA)_4(\mu\text{-}O)_2(\mu_4\text{-}Suc)](ClO_4)_4(OH)_2\cdot 1.5CH_3CN\cdot 2C_2H_5OH\cdot 6H_2O$ (**1**) and $[Fe_4(TBA)_4(\mu\text{-}O)_2(\mu_4\text{-}Tp)](ClO_4)_6\cdot 3C_2H_5OH\cdot 6H_2O$ (**2**) (Suc = succinate, Tp = terephthalate, TBA = tris(2-benzimidazolylmethyl)amine) have been prepared and characterized by various physicochemical techniques. X-Ray crystallography reveals complex **1** contains equivalent two μ-oxo-μ-carboxylate diiron(III) centers bridged by a succinate acting as a tetradentate ligand linked to four iron atoms, forming a tetranuclear core $[Fe_4(TBA)_4(O)_2(Suc)]^{6+}$, in which each iron atom has an N_4O_2 donor set with distorted octahedral geometry and each of the two diiron(III) centers contains two iron atoms with a distinct coordination environment. Magnetic behaviors indicate the presence of a stongly antiferromagnetic coupling in the two complexes with the exchange coupling constants $J = -114.27(8)$ cm^{-1} for **1** and $J = -119.52(6)$ cm^{-1} for **2**. The NMR spectra imply that the structures in the solid state are retained in solution. The two tetranuclear complexes exhibit similar cyclic voltammograms, *i.e.* there are three irreversible two-electron redox peaks at $E_c = 0.247$, -0.233 V; $E_a = 0.354$ V for **1** and $E_c = 0.307$, -0.166 V; $E_a = 0.526$ V for **2**. The preliminary study on the hydrolysis of adenosine 5′-triphosphate (ATP) followed by ^{31}P NMR spectroscopy shows that the two complexes can catalyze the hydrolysis of ATP.

Introduction

Purple acid phosphatases (PAPs) are a group of nonspecific phosphomonoesterases from animal, plant and fungal sources, which are capable of promoting phosphorylation and dephosphorylation, *i.e.* phosphate ester bond-making or -breaking reactions. All of the PAPs characterized to date contain a binuclear metal center [Fe(III)–M(II)]. Mammalian PAP (mPAP) contains a μ-oxo binuclear Fe(III)–Fe(II) metal center, in which the two iron atoms are antiferromagnetically coupled. A role in degradative biological processes, such as in the phagocytosis of aged erythrocytes and in active bone resorption, implicated that the functions for mPAP include phosphoryl transfer and a broad range of hydrolytic reactions. The enzyme is a target for drug design because there is strong evidence for its involvement in bone resorption. However, only in the last few years, has detailed three-dimensional structural information been available for a red kidney bean enzyme, sweet potato and mammalian PAP.[1–4]

Presently, only a few model compounds for purple acid phosphatases, which show phosphatase-like activity, are well documented.[5] Moreover, very few have been investigated for the hydrolysis of adenosine 5′-triphosphate (ATP) as substrate, though this might cast light on the study of the directed cleavage of the nucleic acids RNA and DNA, as well as the understanding of the active sites and model design of phosphatases. In this work, we report the syntheses, structure, NMR spectra and magnetic, spectral, electrochemical properties of two tetranuclear iron complexes containing two μ-oxo diiron(III) centers linked by succinate (Suc) or terephthalate (Tp), $[Fe_4(TBA)_4(\mu\text{-}O)_2(\mu_4\text{-}Suc)](ClO_4)_4(OH)_2\cdot 1.5CH_3CN\cdot 2C_2H_5OH\cdot 6H_2O$ (**1**) and $[Fe_4(TBA)_4(\mu\text{-}O)_2(\mu_4\text{-}Tp)](ClO_4)_6\cdot 3C_2H_5OH\cdot 6H_2O$ (**2**) [TBA = tris(2-benzimidazolylmethyl)amine], as well as a preliminary study on the catalytic hydrolysis toward ATP of the two complexes.

Experimental

Materials

The ligand tris(2-benzimidazolylmethyl)amine was synthesized according to literature procedures.[6] All other chemicals used in this study were commercially available and were used without further purification.

Physical measurements

UV-vis spectra were recorded using a Shimadzu UV-265 spectrometer. IR spectra (4000–400 cm^{-1}) and far-IR spectra (500–100 cm^{-1}) of solid complexes were recorded on a Perkin-Elmer 983 and a Nicolet 170 SX FT-IR spectrometer, respectively. Magnetic susceptibility data were recorded with a Quantum Design superconducting SQUID susceptometer, and diamagnetic corrections to the observed susceptibilities were applied using Pascal's constants. All NMR experiments were performed on a Bruker ARX-500 spectrometer with an inverse probe tuned at 500.13 MHz for ^{1}H, 125.75 MHz for ^{13}C and 202.45 MHz for ^{31}P. Chemical shifts (ppm) were referenced to internal tetramethylsilane (TMS) for ^{1}H and ^{13}C, and 85% H_3PO_4 as external standard for ^{31}P, respectively. The EPR spectra were obtained with a Bruker ER 200D-SRC EPR spectrometer. Electrochemical measurements (cyclic voltammetry and chronocoulometry) were performed with a BAS-100A Electrochemical Analyzer in a conventional three-electrode cell, *i.e.* the working electrode was a glassy-carbon

† Electronic supplementary information (ESI) available: Fig. S1: ^{1}H NMR spectrum of **2** in d_6-DMSO at room temperature. See http://www.rsc.org/suppdata/dt/b3/b303369b/

DOI: 10.1039/b303369b

electrode, a platinum wire was the auxiliary electrode and an Ag/AgCl electrode was the reference electrode. The working electrode was frequently polished with an alumina/water slurry, after which it was washed with water and then with a dimethylformamide (DMF). This cleaning treatment is required to obtain reproducible results, particularly for the reduction processes. The supporting electrolyte tetrabutylammonium perchlorate was recrystallized twice from methanol and dried overnight in vacuum, and the solvent DMF was distilled under vacuum before use. The ferrocene/ferrocenium (Fc/Fc^+) oxidation process was used as a reference standard by frequently measuring the potential for oxidation of a 1.0×10^{-3} mol dm^{-3} solution of ferrocene and all potentials are reported *vs.* Fc/Fc^+.

Syntheses and characterization

$[Fe_4(TBA)_4(O)_2(Suc)](ClO_4)_4(OH)_2\cdot 1.5CH_3CN\cdot 2C_2H_5OH\cdot 6H_2O$ (1). The ligand TBA (0.407 g, 1.0 mmol) in ethanol (20 cm^3) was treated with $Fe(ClO_4)_3\cdot 9H_2O$ (0.511 g, 1.0 mmol) in acetonitrile (20 cm^3). Succinic acid (0.029 g, 0.25 mmol) was added to the resulting red–brown solution, with stirring at room temperature, and triethylamine was added dropwise to adjust the solution pH until the solution turned greenish yellow. After stirring for several hours, the greenish-yellow solution was filtered and the clear filtrate was allowed to undergo slow evaporation at room temperature for about 2 weeks, which led to the deposition of well-formed dark brown crystals which lost solvent molecules quickly on being exposed to the air. The crystalline mass was collected by filtration, washed with diethyl ether and dried in *vacuo* to produce 0.42 g (15.7%) of yellow–green polycrystalline powder. Anal. Calc. for $Fe_4C_{107}H_{118.5}N_{29.5}O_{32}Cl_4$: C, 47.64; H, 4.40; N, 15.32; Fe, 8.29%, Found: C, 47.89; H, 4.20; N, 15.67; Fe, 8.38%. Molar conductivity, Λ_m = 910 S dm^3 mol^{-1} (CH_3CN, 22 °C). IR (KBr disk, cm^{-1}): ~3300 (br s, ν_{N-H}, ν_{C-H}, ν_{O-H}); 1624 (s), 1448 (vs), 1325 (s), 1277 (s), 746 (vs); $\nu_{Fe-O-Fe}$: 756 (m, ν_{as}) and 472 (w, ν_s); $\nu_{CO_2^-}$: 1598 (s, ν_{as}) and 1384 (s, ν_s); $\nu_{ClO_4^-}$: 1098 (vs), 1043 (m), 918 (m), 623 (s). Far-IR (Nujol mull, cm^{-1}): 431 (m) ν_{Fe-O}; 334 (m), 286 (m) ν_{Fe-N}. UV-Vis (CH_3CN): λ_{max}/nm (ε_m/dm^3 mol^{-1} cm^{-1}): 246 (12215), 273 (13303), 280 (12423), 332 (3290), 370 (3182), 425 (516), 480 (413), 496 (317), 604 (44). CV (DMF, scan rate: 200 mV s^{-1}): E_c = 247 mV (i_c = 6.45 μA) and E_c' = −233 mV (i_c' = 5.92 μA); E_a = 354 mV (i_a = 6.20 μA).

$[Fe_4(TBA)_4(O)_2(Tp)](ClO_4)_6\cdot 3C_2H_5OH\cdot 6H_2O$ (2). This was prepared by the same method using terephthalic acid instead of succinic acid. A greenish-yellow polycrystalline power of the complex was obtained by filtration, washed with ethanol and recrystallized from ethanol, and a dark brown crystal formed after two weeks. Unfortunately, it was too efflorescent to be suitable for X-ray diffraction. Anal. Calc. for $Fe_4C_{110}H_{118}N_{28}Cl_6O_{39}$: C, 45.95; H, 4.10; N, 13.65; Fe, 7.78%, Found: C, 46.02; H, 4.44; N, 13.97; Fe, 7.85%. Λ_m = 913 S dm^3 mol^{-1}. IR (KBr disk, cm^{-1}): 3306–2920 (br, s), 1624 (s), 1453 (vs), 1333 (s), 1274 (s), 744 (vs); $\nu_{Fe-O-Fe}$: 702 (s), 467 (w); $\nu_{CO_2^-}$: 1597 (s), 1385 (s); $\nu_{ClO_4^-}$: 1084 (s), 1044 (m), 916 (m), 621 (s). Far-IR: 433 (m); 333 (m), 286 (m). UV-Vis. (DMF) λ_{max}/nm (ε_m/cm^{-1} dm^3 mol^{-1}): 249 (10686), 275 (12260), 283 (12952); 352 (4052), 363 (3610); 422 (3466), 490 (630); 750 (54). CV (in DMF, scan rate: 200 mV s^{-1}): E_c = 307 mV (i_c = 4.44 μA) and E_c' = −166 mV (i_c' = 9.74 μA); E_a = 526 mV (i_a = 9.01 μA).

CAUTION: metal perchlorate salts containing organic ligands are potentially explosive. Only small amounts of material should be prepared, and these should be handled with great care.

X-Ray data collection and refinement

A black, block crystal of size 0.60 × 0.35 × 0.35 mm was mounted on a glass fiber coated with a viscous high-molecular-weight hydrocarbon and used to collect diffraction data at 20 °C on an Rigaku AFC6S four-circle diffractometer with graphite-monochromated Mo-Kα (λ = 0.71069 Å) radiation. The structure was solved using the Patterson methods option of SHELXS-97[7] and developed using conventional alternating cycles of least-squares refinement on F^2 (SHELXL-97)[8] and difference Fourier synthesis. The anions and solvent molecules were refined disordered. For perchlorates, the s.o.f.s of the disordered oxygen atoms were fixed at 0.5. Two sites for ethanol molecules were observed in the asymmetric units, the s.o.f.s were constrained with 0.75 and 0.25, respectively. Two CH_3CN molecules were refined with s.o.f.s = 0.5 and 0.25, respectively. Eight water molecules were found from the difference maps, in which seven were disordered with the s.o.f. = 0.5, 0.5, 0.25, 0.5, 0.5, 0.5, 0.25 for OW2 to OW7, respectively. For charge balance, one of the water molecules should be assumed to be hydroxide.[9] All the non-hydrogen atoms were refined anisotropically. The hydrogen atoms of the ligands were generated geometrically and allowed to ride on their respective parent atoms. The hydrogen atoms of water molecules or hydroxide anions were not determined and refined. The maximum and minimum peaks on the final difference Fourier map are 0.481 and −0.290 e A^{-3}, respectively. Crystallographic data are summarized in Table 1.

Table 1 Crystal data and structure refinement details of complex **1**

Empirical formula	$Fe_4C_{107}H_{118.5}N_{29.5}Cl_4O_{32}$
Formula weight	2695.01
Crystal system	Monoclinic
Space group	*C*2/*c*
a/Å	25.007(5)
b/Å	16.885(3)
c/Å	35.909(7)
β/°	95.36(3)
V/Å^3	15096(5)
Z	4
D_c/g cm^{-3}	1.250
μ/mm^{-1}	0.523
Total/unique reflections (R_{int})	9435/9178 (0.0346)
Observed reflections [$I > 2\sigma(I)$]	4831
R indices [$I > 2\sigma(I)$]	$R1^a$ = 0.0742, $wR2^b$ = 0.1779

^{a} $R1 = \Sigma||F_o| - |F_c||/\Sigma|F_o|$. ^{b} $wR2 = [\Sigma[w(F_o^2 - F_c^2)^2]/\Sigma[w(F_o^2)^2]]^{1/2}$, $w = 1/[\sigma^2(F_o^2) + (0.1654P)^2]$, where $P = (F_o^2 + 2F_c^2)/3$.

CCDC reference number 138830.

See http://www.rsc.org/suppdata/dt/b3/b303369b/ for crystallographic data in CIF or other electronic format.

Results and discussion

Structure description of $[Fe_4(TBA)_4(O)_2(Suc)]^{6+}$ (1)

Selected bond lengths and angles of the complex are given in Table 2. A drawing for the asymmetric center of the cation is shown in Fig. 1, together with the numbering scheme.

Complex **1** crystallizes in the monoclinic space group *C*2/*c*, with the Fe_4 cation lying on the direction of C_2 axis. Through the carboxylate oxygen atoms, the succinate group as a tetradentate ligand is bonded on each side to two iron(III) centers bridged by an oxygen atom, yielding a bridge that runs parallel to the *c*-axis between two μ-oxo diiron(III) groups (Fig. 2). This results in the formation of the tetranuclear iron(III) core, $[Fe_4(TBA)_4(O)_2(Suc)]^{6+}$, in which each iron atom is six-coordinated and possesses an N_4O_2 environment by virtue of three benzimidazolyl nitrogen atoms, one tertiary amine atom from TBA, one oxygen atom from succinate and a bridging oxygen atom with distorted octahedral geometry [such as, N(9), N(11), N(13), N(14) and O(1), O(3) for Fe(1)]. As shown in Fig. 2, the intermolecular metal–metal separations are 3.232, 9.004, 8.909, 9.097 Å for Fe(1) ··· Fe(2), Fe(1) ··· Fe(2A), Fe(1) ··· Fe(1A), Fe(2) ··· Fe(2A), respectively. The two μ-oxo diiron units, bridged by the succinate, form a dihedral angle of 84.3° based on the two Fe–O–Fe planes.

Table 2 Selected bond lengths (Å) and angles (°) for complex **1**

Fe(1)–O(3)	1.791(3)	Fe(2)–O(3)	1.753(3)
Fe(1)–O(1)	1.982(3)	Fe(2)–N(3)	2.081(4)
Fe(1)–N(13)	2.104(3)	Fe(2)–O(2)	2.083(3)
Fe(1)–N(11)	2.094(4)	Fe(2)–N(1)	2.078(3)
Fe(1)–N(9)	2.159(4)	Fe(2)–N(5)	2.110(3)
Fe(1)–N(14)	2.288(4)	Fe(2)–N(7)	2.353(4)
O(3)–Fe(1)–O(1)	99.97(12)	O(3)–Fe(2)–N(3)	105.35(13)
O(3)–Fe(1)–N(13)	95.55(13)	O(3)–Fe(2)–O(2)	98.38(12)
O(1)–Fe(1)–N(13)	105.31(13)	N(3)–Fe(2)–O(2)	88.57(13)
O(3)–Fe(1)–N(11)	93.20(13)	O(3)–Fe(2)–N(1)	104.60(12)
O(1)–Fe(1)–N(11)	102.44(13)	N(3)–Fe(2)–N(1)	88.43(14)
N(13)–Fe(1)–N(11)	148.90(14)	O(2)–Fe(2)–N(1)	156.80(12)
O(3)–Fe(1)–N(9)	174.43(12)	O(3)–Fe(2)–N(5)	107.35(14)
O(1)–Fe(1)–N(9)	85.58(12)	N(3)–Fe(2)–N(5)	147.27(14)
N(13)–Fe(1)–N(9)	82.49(13)	O(2)–Fe(2)–N(5)	85.53(12)
N(11)–Fe(1)–N(9)	86.95(14)	N(1)–Fe(2)–N(5)	84.62(13)
O(3)–Fe(1)–N(14)	95.74(12)	O(3)–Fe(2)–N(7)	177.24(13)
O(1)–Fe(1)–N(14)	164.17(13)	N(3)–Fe(2)–N(7)	74.56(14)
N(13)–Fe(1)–N(14)	74.88(14)	O(2)–Fe(2)–N(7)	78.86(12)
N(11)–Fe(1)–N(14)	74.58(14)	N(1)–Fe(2)–N(7)	78.16(13)
N(9)–Fe(1)–N(14)	78.72(13)	N(5)–Fe(2)–N(7)	72.72(14)
Fe(2)–O(3)–Fe(1)	131.55(15)		

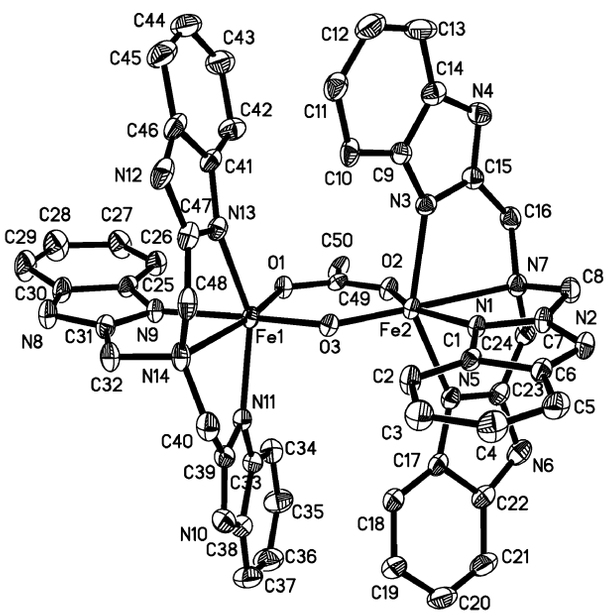

Fig. 1 ORTEP drawing of the asymmetric unit of the cation, $[Fe_4(O)_2(TBA)_4(Suc)]^{6+}$, of complex **1**, with the atom-numbering scheme.

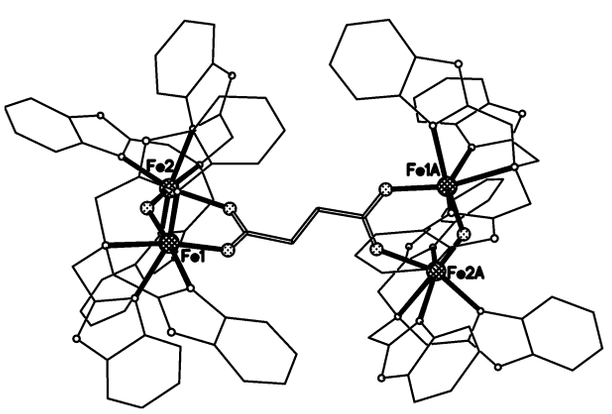

Fig. 2 A perspective view of the cation, $[Fe_4(O)_2(TBA)_4(Suc)]^{6+}$, showing the bridging mode of μ_4-succinate. Anions, solvent molecules and all hydrogen atoms are omitted for clarity. Symmetry transformations used to generate equivalent atoms: A $-x, y, -z + 0.5$.

Each of the two diiron(III) centers contains two iron atoms with a distinct coordination environment, and the TBA ligands have two different orientations (Fig. 1). At the Fe(2) site the tertiary amine nitrogen atom N(7) is *trans* to the oxo-bridge and the *cis* site is occupied by a benzimidazolyl nitrogen atom N(1), while at the Fe(1) site the situation is reversed, the tertiary amine nitrogen atom N(14) is *cis* to the oxo-bridge and a benzimidazolyl nitrogen atom N(9) is *trans* to the oxo-bridge, which is similar to the coordination found in $[Fe_2O(O_2CMe)L^2_2]^{3+}$ (where L^2 is the 1-methyl derivative of TBA)[10a] and $[Fe_2O(O_2CMe)(TPA)]^{3+}$ (TPA = tris(2-pyridylmthyl)amine).[10b] The Fe(1)–N(benzimidazole) average bond length is 2.119 Å and Fe(1)–N(14) (amine) is 2.288 Å, while the Fe(2)–N(benzimidazole) average bond length is 2.090 Å and Fe(2)–N(7)(amine) is 2.353 Å, which also manifests that the coordination environments around the two iron(III) atoms differ markedly. The Fe–N(benzimidazole) bond lengths ranging from 2.078(3) to 2.159(4) Å are obviously shorter than the Fe–N(amine) bond lengths. This is due to the fact that the benzimidazole groups are good σ donors and π acceptors compared to amine and bonded more strongly to iron centers. In addition, the Fe(2)–N(7) bond is longer than Fe(1)–N(14), while the Fe(2)–N(1) bond is shorter than Fe(1)–N(9). This is the result of a significant *trans* influence of the μ-oxo group. Moreover, the Fe–O(oxo) bond lengths [Fe(1)–O(3), 1.791(3) Å and Fe(2)–O(3), 1.753(3) Å] are shorter than the corresponding values observed in doubly bridged diiron(III) analogues,[10] and the Fe–O(oxo) distances differ observably within **1** (Δ(Fe–O(oxo)) = 0.038 Å), which should also be due to the *trans* influence of *trans*-groups. For Fe(1) and Fe(2), the large deviations of bond angle from 90° of the idealized octahedral geometry are found for angles N(13)–Fe(1)–N(14) [74.88(14)°], N(11)–Fe(1)–N(14) [74.58(14)°], N(5)–Fe(2)–N(7) [72.72(14)°] and N(3)–Fe(2)–N(7) [74.56(14)°]. As mentioned above, the Fe(1) ··· Fe(2) separation is 3.232 Å, shorter than those found in the μ-oxo-μ-carboxylato dibridged iron(III) complexes. Additionally, the Fe(1)–O(3)–Fe(2) angle of 131.55(15)° is slightly bigger than those in diiron(III) analogues.[10] This is probably caused by the bridging ligand succinate, which links the two diiron(III) centers to pull them together, thus causing the change of the coordination sphere of the two iron atoms and related bond lengths and angles.

Magnetic susceptibilities

Variable-temperature (5–300 K) magnetic susceptibility data were collected on polycrystalline samples for both the complexes in a 1.0 T field. A plot of the molar magnetic susceptibilities (χ_M) of the two compounds in the range of 5–300 K are shown in Fig. 3. The effective magnetic moment (μ_{eff}) per Fe decreases gradually from 1.68 (1.77) μ_B at 300 K to 0.27 (0.53) μ_B at 5 K for **1** (**2**), which imply that there is a strongly antiferromagnetic coupling interaction within the two diiron(III) centers. We attempted to interpret these magnetic systems of

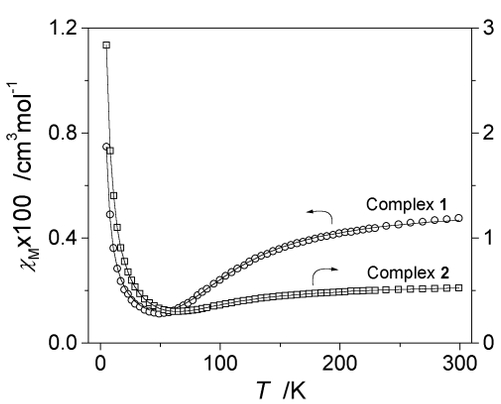

Fig. 3 Molar susceptibility (per mole complex) as a function of temperature (5–300 K) for complexes **1** and **2**. The solid lines result from a nonlinear least-squares fitting to the theoretical expression for all experimental data as indicated in the text.

both the complexes by use of the Heisenberg–Dirac–van Vleck spin Hamiltonian ($H = -2JS_1S_2$) for a spin-coupled dimer model with an $S_1 = S_2 = 5/2$ basis set.[11] For the two μ-oxo-μ-carboxylato diiron centers [Fe(1) ··· Fe(2) and Fe(1A) ··· Fe(2A)], there should be a different J values. However, to the first approximation, they are regarded as equivalent. Considering the exchange interactions between two diiron centers through bridging succinate or terephthalate groups, a molecular field (zJ')[10] was added to account approximately for the actual nature of the two complexes. Then, the molar susceptibilities for the two complexes can be given as:

$$\chi = \frac{2Ng^2\beta^2(2e^{2x} + 10e^{6x} + 28e^{12x} + 60e^{20x} + 110e^{30x})}{kT(1 + 3e^{2x} + 5e^{6x} + 7e^{12x} + 9e^{20x} + 11e^{30x})} \quad (1)$$

$$\chi' = \chi/(1 - 2zJ'\chi/Ng^2\beta^2) \quad (2)$$

$$\chi_M = (1 - P)\chi' + 4P\chi_{para} + TIP \quad (3)$$

where $x = J/kT$, P = mole percentage of paramagnetic impurity/100, TIP = temperature-independent paramagnetism, $\chi_{para} = (S)(S + 1)(Ng^2\beta^2/3k\mathrm{T})$, J is the exchange coupling constant within the two diiron centers and zJ' is the cross coupling constant for the interaction between the two diiron centers; N, k, β and T have their usual meanings. Nonlinear least-squares fitting of the above-mentioned model to the experimental data have been made by varying J, P, TIP and zJ', and minimizing the residual $R = [\Sigma(\chi_{obs} - \chi_{calc})^2/n\Sigma(\chi_{obs})^2]$ (where n is the number of experimental data, 59). A reasonable fit was obtained for the 5–300 K data with g fixed at 2.0, yielding the following parameters: $J = -114.27(8)$ cm^{-1}, $P = 2.16(9) \times 10^{-3}$, TIP = 4.95×10^{-5} emu mol^{-1}, $zJ' = -8.76(1)$ cm^{-1} with residual $R = 2.00 \times 10^{-7}$ for complex **1** (as shown in Fig. 3); and $J = -119.52(6)$ cm^{-1}, $P = 8.20(4) \times 10^{-3}$, TIP = 4.50×10^{-4} emu mol^{-1}, $zJ' = -7.66(1)$ cm^{-1}, $R = 1.28(5) \times 10^{-6}$ for complex **2**. The exchange interaction parameters in other reported μ-oxo-μ-carboxylato doubly bridged iron(III) complexes range from −108 to −118 cm^{-1}. The values of J found here essentially fall in the range and indicate the presence of strongly antiferromagnetic coupling interactions in the two diiron centers. Besides, the zJ' values show that there are only weak antiferromagnetic interactions between the two diiron centers.

NMR spectra

^{1}H spectra of the two complexes and 2D ^{1}H–^{13}C HMQC NMR spectrum of **1** were performed in d$_6$-DMSO in order to elucidate the solution structure of the complexes and are shown in Fig. 4 and Fig. S1 (ESI †), respectively.

It can be seen that all of the signals appear within the range 0–20 ppm and have good resolution, and the two compounds exhibit nearly the same patterns (see Fig. 4). Compared with the ^{1}H spectra of those dibridged diiron(III) analogues,[10,12] all of the peaks are sharper and shift to higher field, indicating that there exists stronger antiferromagnetic coupling within the Fe$_4$ cluster. This agrees with the results of magnetic susceptibility discussed above and implies that the structures for the two complexes in the solid state are retained in solution.

In the crystal structure of complex **1**, the average distances of the benzimidazolyl C2, C3, C4 and C5 to iron centers are 3.87, 5.22, 5.93 and 5.61 Å, respectively. So, the peaks at 5.2, 5.4, 5.7 and 5.9 ppm with ^{13}C shift at *ca.* 131 ppm can be assigned to benzimidazolyl C^2 protons (Bzim C^{2}H) due to its broadest resonances and shortest distance to iron centers. Then, the broader peak at 7.0 ppm with ^{13}C shift at 167 ppm is assigned to benzimidazolyl C^3 protons (Bzim C^{3}H). The other five peaks at 6.2, 6.3, 6.6, 6.7 and 7.6 ppm with ^{13}C shift in the range 127–155 ppm can be assigned to benzimidazolyl C^4 or C^5 protons (Bzim C^{4}H or C^{5}H). In comparison with the ^{1}H NMR spectra of μ-oxo diiron(III) complexes with the TBA ligand,[10a,12] the four broad, poorly resolved signals at 10.8, 11.1, 11.3 and 11.7 ppm should arise from the benzimidazolyl NH protons (Bzim NH). The complexity of these features demonstrates the complex contains spectroscopically distinct iron centers in solution. In the lowest field, the broadest resonances at 18.6 ppm for **1** and 17.8 ppm for **2** can be assigned to the methylene protons of TBA ligands (NCH_2) with an average distance of 3.08 Å to iron atoms for **1**. In addition, two very broad and weak signals are observed at 9.2 and 15.6 ppm for **1** and 7.4, 8.3 ppm for **2**, which are probably attributed to –CH_2CH_2– of succinate and phenyl-ring protons of terephthalate, respectively. It is noteworthy that these groups of protons displaying two peaks suggest the exogenous bridge ligands, succinate and terephthalate, are rigid and can not rotate freely. Therefore, the structure of μ-oxo diiron centers strapped by succinate and terephthalate in the crystal persists in solution.

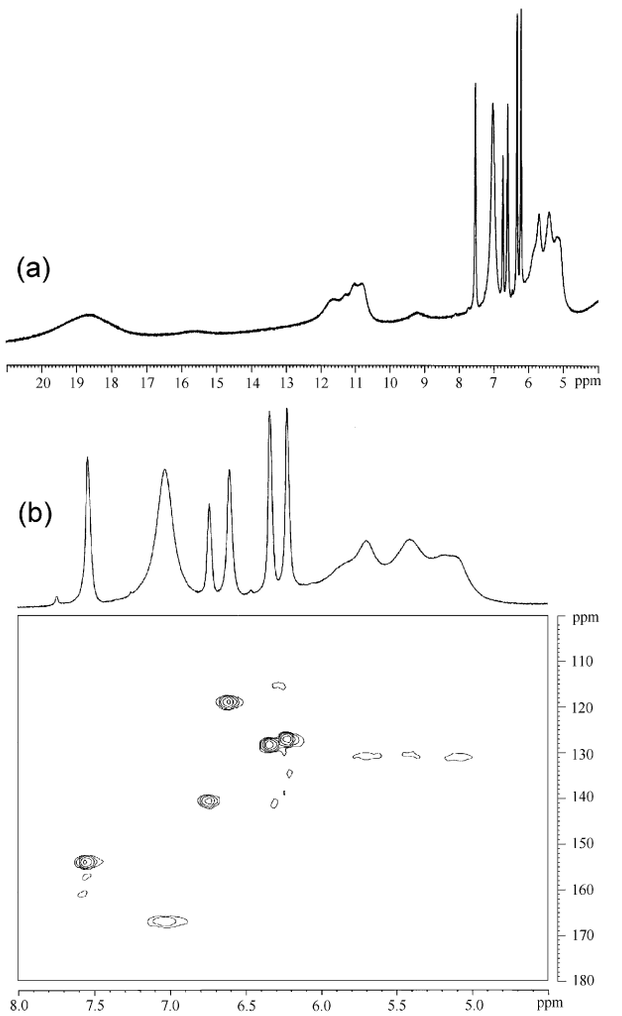

Fig. 4 (a) ^{1}H NMR and (b) ^{1}H–^{13}C HMQC NMR spectra of complex **1** in d$_6$-DMSO at room temperature.

UV-vis spectra

The two complexes exhibit similar UV-vis features, which are also similar to those of reported μ-oxo-μ-carboxylato dibridged diiron complexes. In the higher energy region, there are several well-resolved strong bands, which are assigned to carboxylate → Fe(III) transition near 250 nm, π → π* of benzimidazolyl rings of the ligands near 280 nm and μ-oxo → Fe(III) charge-transfer transitions in the range 330–390 nm. Shoulder peaks are apparent in 400–500 nm region, which are attributed to $^6A_1 \rightarrow [^4E, {}^4A_1]$ (^{4}G) ligand field transitions enhanced by nearby oxo LMCT bands.[13] Broad bands occur at 604 or 750 nm (ε_m <100 dm^3 mol^{-1} cm^{-1}), which are assigned to the $^6A_1 \rightarrow {}^4T_2$ (^{4}G) ligand field transition.

IR spectra

The infrared spectra of these compounds show two strong features at *ca.* 1598, 1384 cm^{-1}, which are assigned to asymmetric and symmetric vibrations of the μ-carboxylate groups of succinate or terephthalate, and the frequency differences are in accord for carboxylato bridged coordination. The Fe–O–Fe asymmetric stretches are assignable at 756 and 702 cm^{-1}, while the symmetric stretches are tentatively assigned at 472 and 467 cm^{-1}, for **1** and **2**, respectively, which are typical values for μ-oxo bridged diiron(III) centers.[14] Two strong peaks occur near 1100 cm^{-1} and 623 cm^{-1}, indicating the perchlorate ions are uncoordinated. The strong and broad bands near ~3300 cm^{-1} arise from the O–H stretching vibrations of lattice water or ethanol and the N–H and C–H stretching vibrations of the aromatic rings. The bands at 1624 and 746 cm^{-1} correspond to skeletal and folding vibrations of the aromatic ring, respectively; the bands near 1325 and 1277 cm^{-1} are the third amino and aliphatic C–N vibration, respectively. In the two complexes, the bands at 1448 and 1453 cm^{-1} for **1** and **2**, respectively, imply direct coordination of the benzimidazolyl nitrogen to iron.

EPR spectra

The X-band EPR spectra of the two complexes in DMF solution are nearly EPR silent at 110 K, which are consistent with two antiferromagnetically coupled diiron(III) centers.

Electrochemistry

Cyclic voltammograms of the two tetranuclear complexes in DMF solution were recorded in potential range of +1.0 to −0.6 V under a nitrogen atmosphere (Fig. 5). They exhibit very similar patterns, *i.e.* there are successive two cathodic peaks at E_c = 0.260 V (*vs.* Ag/AgCl) (i_c = 4.23 μA), E_c' = −0.219 V (i_c' = 4.10 μA) for **1** and E_c = 0.307 V (i_c = 3.18 μA), E_c' = −0.154 V (i_c' = 6.38 μA) for **2**, as well as an anodic peak E_a = 0.356 V (i_a = 3.75μA) for **1** and E_a = 0.513 (i_c = 6.53 μA) for **2**, at a scan rate of 100 mV s^{-1}. The values of $i_p/\sqrt{v}$ of each peak are almost constant when scan rates were (v) increased between 40–250 mV s^{-1}, which suggest that the three electrode processes are diffusion controlled. The electron number of each step is given by calculating the peak integrated area from the cyclic voltammogram and according to the following equation as well as from straight line plots of Q *vs.* $\sqrt{t}$ in chronocoulometry measurements:[15]

$$Q = \frac{2nFAC\sqrt{Dt}}{\sqrt{\pi}}$$

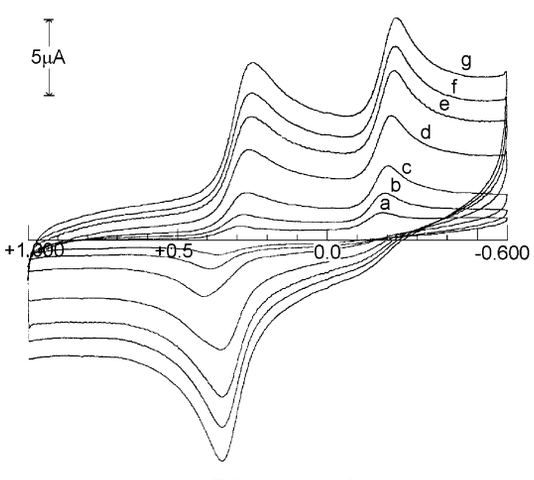

Fig. 5 Cyclic voltammograms of complex **1** (c = 1 mmol dm^{-3}) in DMF and with various scan rates (mV s^{-1}): (a) 10, (b) 20, (c) 40, (d) 100, (e) 160, (f) 200, (g) 250.

where Q is the amount of charge in coulombs that has passed at time, t, since the application of the potential step; C and D are the concentration and diffusion coefficients of the reactants, respectively, A is the electrode area; and n and F have their usual significance. The three irreversible electrode reactions are all consistent with a two-electron process. Thus, the first cathodic peak should correspond to reduction reaction $2Fe(III)_2 \longrightarrow 2Fe(III)Fe(II)$; and the second cathodic peak is for the further reduction reaction: $2Fe(III)Fe(II) \longrightarrow 2Fe(II)_2$; then the anodic peak represents the reverseprocess: $2Fe_2(II) \longrightarrow 2Fe(III)Fe(II)$.

Preliminary study on the catalysis to ATP-hydrolysis

Hydrolysis of Na_2H_2ATP was promoted by the two complexes in D_2O–H_2O (v/v = 1 : 9) solution under various reaction conditions. Since most ^{31}P NMR signals of ATP, ADP, AMP, pyrophosphate (P–P) and orthophosphate (Pi) are distinct, ATP hydrolysis can be monitored conveniently by following the change in concentration of various hydrolytic products with time by signal integration of T_α, T_β and T_γ (for the α-, β- and γ-phosphate groups of ATP), with chemical shifts (δ) at −8.7, −20.7 and −8.1 ppm, respectively. Similarly, D_α and D_β (α- and β-phosphate of ADP) and sum of orthophosphate (Pi, δ +3.3 ppm) and AMP (δ +2.9 ppm), although these signals are often overlapped, *e.g.* T_α and D_α, T_γ and D_β as well as Pi and AMP. The assignment of peaks is based on the literature.[16] Fig. 6 shows ^{31}P NMR spectra for ATP hydrolysis after 2 h. Because of the presence of paramagnetic iron(III)-containing complexes in the reaction mixture, the peaks are broadened and the four peaks T_α, T_β, D_α and D_β can not be separated distinctly. On the other hand, the peaks for the two compounds are only slightly broadened, indicating that the concentration of paramagnetic impurities in the system is very low. In Fig. 6, no signal for pyrophosphate (P–P) is observed, but the signals for ATP, ADP, AMP and Pi, imply that the products of ATP-hydrolysis are orthophosphate and ADP, which subsequently produces AMP and Pi, *i.e.* the hydrolysis process can be described as: ATP–Pi ⟶ ADP–Pi ⟶ AMP. There is no evidence to demonstrate the hydrolysis of the produced AMP (AMP–Pi ⟶ adenosine) and the release of pyrophosphate (δ = 9.70 ppm) at pH 3.0 and 18 °C. This indicates that these di- and tetra-ferric compounds

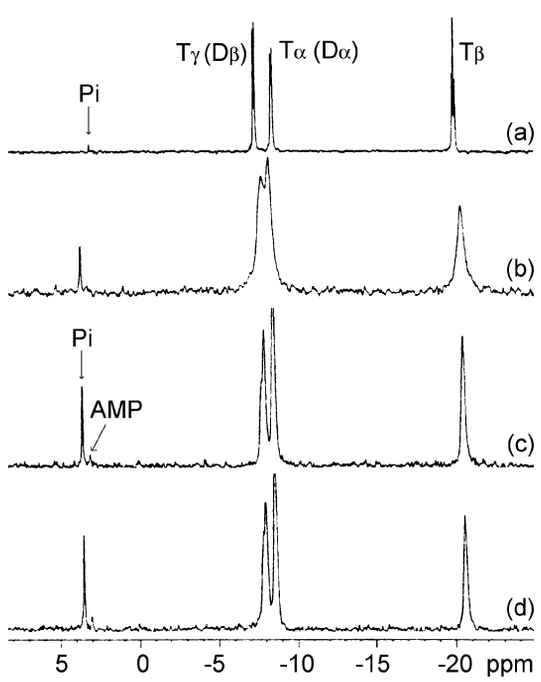

Fig. 6 ^{31}P NMR spectra of ATP-hydrolysis products catalyzed by different complexes (0.45 mmol dm^{-3}) after 2 h at pH *ca.* 3.0 and 18 °C: (a) pure ATP, (b) Fe_2(DTPB)(μ-OH)(μ-Ac)Cl_4·$5H_2O$, (c) [Fe_4(TBA)$_4$(μ-O)$_2$(μ$_4$-Suc)](ClO$_4$)$_4$(OH)$_2$·$1.5CH_3CN$·$2C_2H_5OH$·$6H_2O$, (d) [Fe_4(TBA)$_4$(μ-O)$_2$(μ$_4$-Tp)](ClO$_4$)$_6$·$3C_2H_5OH$·$6H_2O$.

Table 3 The pseudo-first-order rate constants and molar turnover numbers for ATP-hydrolysis catalyzed by the two complexes

Complex	T/°C	pH	$[ATP]_0$ /mM	[Comp] /mM	t/min	10^3k/min^{-1}	η/min^{-1}
1	18	3.0	25.0	0.45	120	2.31	0.112
	17	5.0	23.6	0.33	30	1.20	0.084
	17	4.0	26.3	0.21	20	2.32	0.284
	37	2.0	30.3	0.21	15	3.96	0.554
	37	1.5	30.3	0.21	13	6.63	0.917
	37	1.0	324.3	0.21	10	9.89	14.547
2	18	3.0	25.0	0.45	120	3.29	0.151
	17	5.0	23.6	0.33	30	3.07	0.210
	17	4.0	26.3	0.21	20	7.12	0.832
	37	2.0	30.3	0.21	20	7.70	1.029
	37	1.5	30.3	0.21	22	8.22	1.085
	37	1.0	324.3	0.21	20	10.80	15.010

only catalyze the exo-cleavage of phosphoanhydride bond and can not catalyze intra-cleavage of phosphoanhydride and phosphoester bonds.

Provided that the spontaneous primary and secondary hydrolysis of ATP in acidic solution is negligible,[17] the pseudo-first-order rate constant k for ATP hydrolysis is:

$$-\frac{\mathrm{d}[\mathrm{ATP}]}{\mathrm{d}t} = k[\mathrm{ATP}]$$

This equation is integrated to obtain the equation:

$$\ln\frac{[\mathrm{ATP}]_0}{[\mathrm{ATP}]_t} = kt$$

and the molar turnover number η:

$$\eta = \frac{[\mathrm{Pi}]_t}{[\mathrm{Comp}]_0 t}$$

where [ATP], [Pi] and [Comp] are the concentrations of ATP, inorganic phosphate and complex, respectively; t is the reaction time. Then, the rate constants and the molar turnover numbers of catalytic hydrolysis under various conditions (temperature, pH value and substrate concentration *etc.*) can be obtained and are shown in Table 3. The rate constants and molar turnover numbers increase as the reaction temperature and the acidity of reaction solution are increased. The hydrolytic rate at 18 °C and pH *ca*. 3 for both complexes are more than twice that of the similar binuclear complex, Fe_2(DTPB)(μ-OH)(μ-OAc)Cl_4·$5H_2O$[18] [DTPB = 1,1,4,7,7-penta(2-benzimidazolylmethyl)-diethylenetriamine] (see Fig. 6).

Conclusion

We have synthesized two new tetranuclear iron(III) complexes containing two μ-oxo diiron(III) centers bridged with succinate or terephthalate, which act as a tetradentate ligand linked to four iron(III) atoms. The magnetic results indicate the presence of strong antiferromagnetic interaction in the μ-oxo diiron moieties and weak antiferromagnetic interactions between the two diiron centers through the μ_4-bridging ligand, succinate or terephthalate. The NMR studies indicate that the structures existing in solid state are also retained in solution. The two complexes can promote the hydrolysis of ATP.

Acknowledgements

This project was founded by National Natural Science Foundation of China, and partially supported by the State Key Laboratory for Structure Chemistry of Unstable & Stable Species in Peking University, the Laboratory of NMR & Atomic Molecular Physics in Wuhan Institute of Physics and Mathematics, and the State Key Laboratory of Coordination Chemistry in Nanjing University.

References and notes

1 N. Sträter, W. N. Lipscomb, T, Klabunde and B. Krebs, *Angew. Chem., Int. Ed. Engl.*, 1996, **35**, 2024.
2 L. W. Guddat, A. S. McAlpine, D. Hume, S. Hamilton, J. de Jersey and J. L. Martin, *Structure*, 1999, **7**, 757.
3 N. Sträter, T. Klabunde, P. Tucker, H. Witzel and B. Krebs, *Science*, 1995, **268**, 1489.
4 G. Schenk, C. L. Boutchard, L. E. Carrington, C. J. Noble, B. Moubaraki, K. S. Murray, J. de Jersey, G. R. Hanson and S. Hamilton, *J. Biol. Chem.*, 2001, **276**, 19084.
5 (*a*) P. Karsten, A. Neves, A. J. Bortoluzzi, M. Lanznaster and V. Drago, *Inrog. Chem.*, 2002, **41**, 4625; (*b*) M. Lanznaster, A. Neves, A. J. Bortoluzzi, B. Szpoganicz and E. Schwingel, *Inorg. Chem.*, 2002, **41**, 5641.
6 H. M. J. Hendriks, P. J. M. W. L. Birkers and J. van Rijn, *J. Am. Chem. Soc.*, 1982, **104**, 3607.
7 G. M. Sheldrick, SHELXS-97: A Program for Crystal Structure Solution, Univ. of Göttingen, Germany, 1999.
8 G. M. Sheldrick, SHELXL-97: Crystal Structure Refinement, Univ. of Göttingen, Germany, 1999.
9 An example for the assumption: J. H. Satcher, Jr., M. M. Olmstead, M. W. Droege, S. R. Parkin, B. C. Noll, L. May and A. L. Balch, *Inorg. Chem.*, 1998, **37**, 6751.
10 (*a*) S. Wang, Q. Luo, X. Wang, L. Wang and K. Yu, *J. Chem. Soc., Dalton Trans.*, 1995, 2045; (*b*) R. E. Norman, S. Yan, L. Que Jr., G. Backer, J. Ling, J. Sanders-Loehr, J. H. Zhang and C. J. O'Connor, *J. Am. Chem. Soc.*, 1990, **112**, 1554; (*c*) S. Yan, D. D. Cox, L. L. Pearce, C. Juarez-Garcia, L. Que, Jr., J. H. Zhang and C. J. O'Connor, *Inorg. Chem.*, 1989, **28**, 2507.
11 C. J. O'Connor, *Prog. Inorg. Chem.*, 1982, **29**, 203.
12 A. P. Ginsberg and M. E. Lines, *Inorg. Chem.*, 1972, **11**, 2289.
13 R. M. Buchnan, R. J. O'Brien, J. F. Richardson and J.-M. Latour, *Inorg. Chim. Acta*, 1993, **214**, 33.
14 J. Sanders-Loehr, W. D. Wheeler, A. K. Shiemke, B. A. Averill and T. M. Loehr, *J. Am. Chem. Soc.*, 1989, **111**, 8084.
15 F. C. Anson, *Anal.Chem.*, 1966, **38**, 54.
16 M. W. Hosseini, J. M. Lehn and M. P. Mertes, *Helv. Chim. Acta*, 1993, **66**, 2454.
17 In fact, the spontaneous hydrolysis and the second hydrolysis of ATP can not be negligible in our system. The obtained parameters here are just for a reference.
18 C. Liu, S. Yu, D. Li, Z. Liao, X. Sun and H. Xu, *Inorg. Chem.*, 2002, **41**, 913.